Force and Pressure Measurements on an Airfoil Oscillating through Stall

A.G. Parker*
Texas A&M University, College Station, Texas

Details of force, moment, and pressure distributions on a two-dimensional, 4-ft chord, NACA 0012 airfoil, oscillating in pitch through stall, in a 7 ft × 10 ft low-speed wind tunnel are presented. Tests were run with the airfoil in a closed test section and also in a test section having four longitudinal slots in each sidewall set to provide minimum tunnel interference on the wing in steady flow. In steady flow, differences between the results for the closed and 2% open case are small. The dynamic stall process is not triggered by the bursting of a laminar separation bubble but rather by the separation of the turbulent boundary layer downstream of the bubble.

Nomenclature

c = wing chord
C_M = pitching moment coefficient about the quarter chord
C_N = normal force coefficient
C_P = pressure coefficient
f = frequency of oscillation, Hz
K = nondimensional frequency parameter = $\omega c/2U$)
R_N = Reynolds number
U = wind velocity
x = distance in the chordwise direction measured from the nose of the airfoil
α = angle of attack
ω = angular frequency

Introduction

With the continuing development of high-performance helicopters, problems associated with blade stall flutter have become of increasing concern. This arises in forward flight because the retreating blade has to operate at higher angles of attack than the advancing blade in order to maintain equilibrium in roll. Often these angles are above the static stall angle of the airfoil section. Because of the oscillatory nature of the angle of attack variation through each blade revolution, the stall angle is delayed to well above static stall angles and this causes the stall, when it occurs, to be much more violent than in steady flow. This phenomenon is known as dynamic stall.

Despite the amount of effort that has been spent on this problem (some of which is presented in Refs. 1-8), the mechanisms and flows leading to dynamic stall are still not fully understood. For some time it was felt by several workers[1,4,8] that the stall mechanism was closely linked with the behavior of the leading-edge laminar separation bubble, but recent developments[9] throw considerable doubt on this theory. It was based on a belief in the "leading-edge bubble concept" that the current program of experimental work was undertaken. Because of the small size of the laminar separation bubble, tests were required using larger models which led to large tunnel interference that could not be allowed for in oscillatory testing through stall.

In steady flow, tunnel interference can be reduced significantly by the use of slotted tunnel walls.[10,11] Initial tests, therefore, were conducted to ascertain the best slot configuration to reduce the required corrections on a 4-ft chord two-dimensional NACA 0012 wing.[12] It was assumed that this self correcting of the tunnel would also be valid for unsteady tests in the range of frequencies considered. The program was then planned to obtain detailed pressure measurements on the 4-ft chord wing oscillating in pitch and to compare data in a closed tunnel with that obtained in a tunnel where the walls were slotted for minimum corrections. It is the results of these tests that are given here.

Received Aug. 6, 1975; revision received April 23, 1976. This work was sponsored by NASA Ames Research Center, under Contract NAS2-7917.

Index categories: Nonsteady Aerodynamics; Rotary Wind Aerodynamics.

*Assistant Professor, Aerospace Engineering Dept. Member AIAA.

Equipment and Tests

All tests were conducted in the Texas A&M University's 7 ftx10 ft low speed wind tunnel, using a two-dimensional NACA 0012 airfoil which was pivoted at its quarter chord and could be oscillated in pitch using a variable speed electric motor (Fig. 1). Initial tests to measure the normal force coefficient C_N and the quarter chord pitching moment coefficient C_M required the installation of ten Validyne DP9 pressure transducers connected between the upper and lower surfaces of the wing at several chordwise locations (Table 1). Outputs from these transducers were fed through an operational amplifier summing circuit[2,13] to give output voltages directly proportional to C_N and C_M. These outputs were then recorded on a Honeywell Visicorder along with the angle of attack α of the airfoil.

The solid sidewalls of the tunnel were removed and replaced with walls having four longitudinal slots the width of which could be varied (Fig. 2). Early tests[12] indicate that tunnel

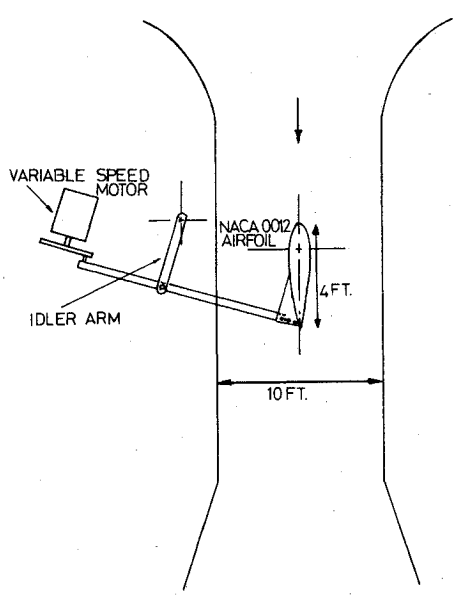

Fig. 1 Schematic of test equipment.

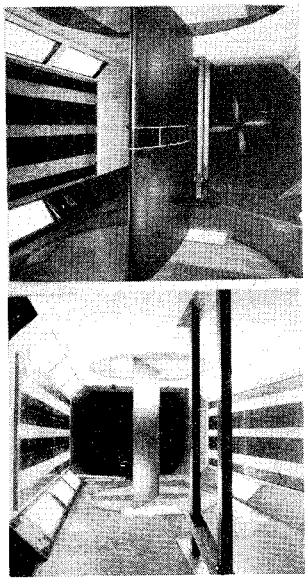

Fig. 2 Details of test equipment.

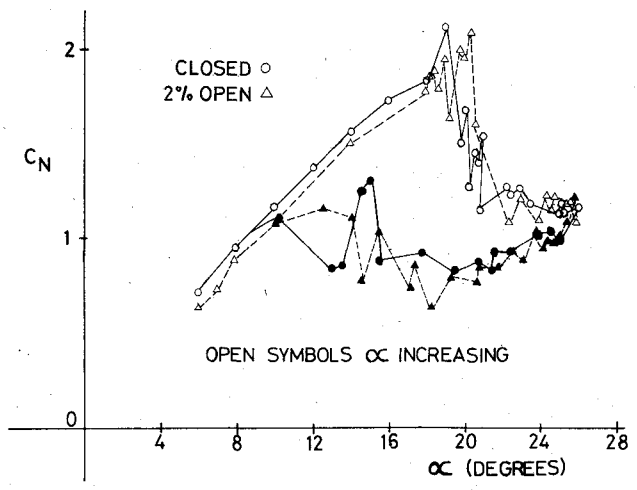

Fig. 3 C_N vs $\alpha K = 0.022$, $R_N = 2 \times 10^6$.

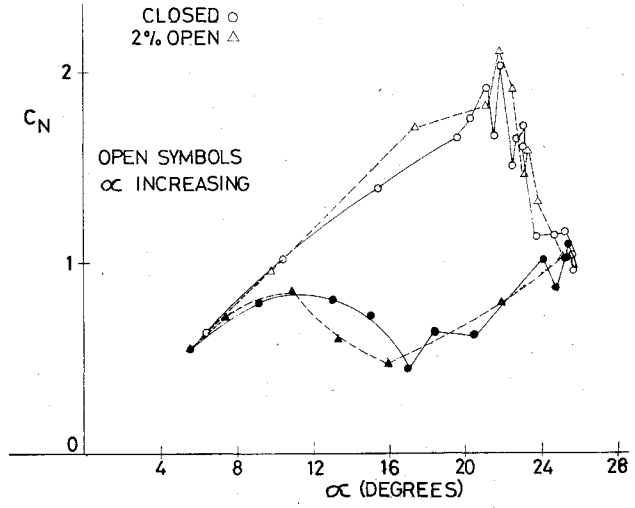

Fig. 4 C_N vs $\alpha K = 0.05$, $R_N = 2 \times 10^6$.

corrections could be minimized with the sidewalls set for 2% open. All subsequent tests were performed for the tunnel sidewalls both closed and 2% open. Oscillatory tests were conducted at three Reynolds numbers (R_N), 1 × 10^6, 2 × 10^6, and 3 × 10^6, and for four frequency parameters, $K = (\omega c/2U)$, of 0.022, 0.05, 0.065, and 0.15. In each case,

Table 1 Transducer locations for force measurements[a]

No.	Location x/c	No.	Location x/c
1	0.025	6	0.30
2	0.05	7	0.40
3	0.10	8	0.60
4	0.15	9	0.70
5	0.20	10	0.90

[a] All transducers connected between the upper and lower surfaces.

Table 2 Transducer locations for pressure measurements[a]

Upper surface		Lower surface	
No.	Location x/c	No.	Location x/c
1	0	13	0.001
2	0.001	14	0.0125
3	0.005	15	0.1
4	0.0125	16	0.2
5	0.025	17	0.3
6	0.05	18	0.4
7	0.1	19	0.6
8	0.2	20	0.9
9	0.3		
10	0.4		
11	0.6		
12	0.9		

[a] All transducers referenced to tunnel static.

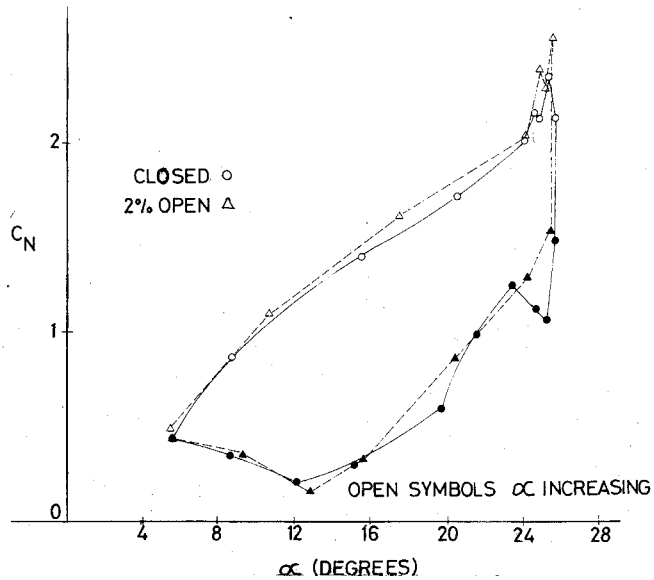

Fig. 5 C_N vs $\alpha K = 0.15$, $R_N = 2 \times 10^6$.

the angle of attack was varied sinusoidally about a mean angle of 16° with an amplitude of ±10°. Data were obtained for several cycles and for each a "typical" cycle was chosen and the data plotted in the form of curves of $C_N - \alpha$ and $C_M - \alpha$. Results obtained for $R_N 2 \times 10^6$ are presented in Figs. 3-8.

As well as overall forces and moments, detailed pressure distributions were measured. To do this, ten more transducers were installed in the wing. Of the twenty transducers, twelve were connected to the upper surface and eight to the lower surface (Table 2). The reference sides of all these transducers were connected to a plenum in the wing which was held at freestream static pressure. Outputs from all the transducers were recorded individually on visicorders to give time histories of the pressure at each location (Fig. 9). Pressure data were obtained for all the previous configurations and again results for "typical" cycles were carpet plotted in the form of the pressure coefficient C_p vs x/c, vs α. Figure 10 was obtained at $R_N = 2 \times 10^6$, $K = 0.15$ for the tunnel 2% open, and is typical.

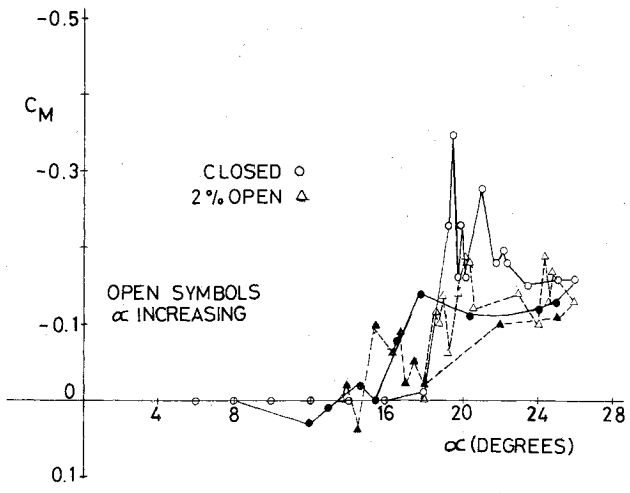

Fig. 6 C_M vs α $K = 0.022$, $R_N = 2\text{x}10^6$.

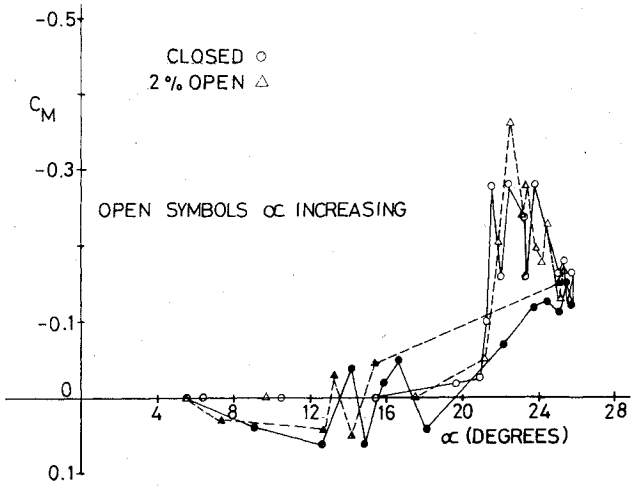

Fig. 7 C_M vs α $K = 0.05$, $R_N = 2 \times 10^6$.

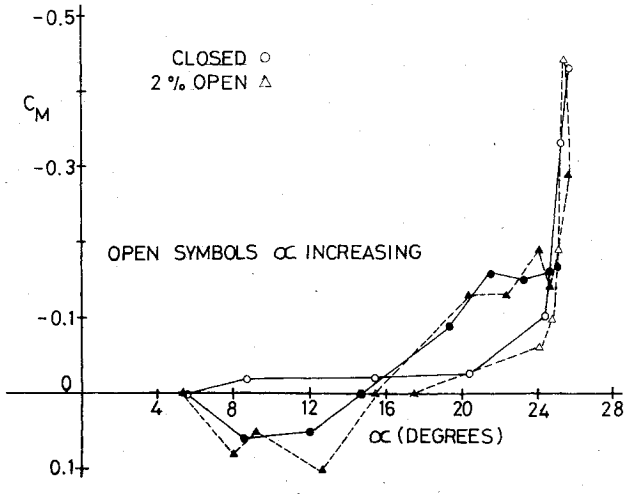

Fig. 8 C_M vs $\alpha K = 0.15$, $R_N = 2 \times 10^6$.

Discussion

In all the tests there was considerable variation in the recorded data from cycle to cycle because the stall process was not identical each time. Averaging result over several cycles might, however, result in a loss of definition of the sharp peaks caused by vortex shedding that occurs in all cycles, but at slightly different points in each cycle. For each test, therefore, a "typical" was chosen and the data presented here.

A. $C_N - \alpha$

Typical results for the low-frequency parameter ($K = .022$) are presented in Fig. 3. The angle of attack for lift stall varies from 19 to 21.5° for Reynolds numbers increasing from 1 to 3 million. Full recovery from the stall occurred at all Reynolds numbers when the angle of attack had decreased to about 12°.

For $K = 0.05$ (Fig. 4), the angle of lift stall has increased slightly (21 to 22° depending on Reynolds number) causing an increase in C_N max. Also the angle of attack for lift recovery has decreased to 10° and it shoud be noted that the minimum value of C_N no longer occurs at the minimum angle of attack.

These trends of increasing stall angle and C_N max with increasing frequency parameter continue for $K = 0.065$ and $K = 0.15$ (Fig. 5), but at $K = 0.15$ the lift stall angle is the same for all Reynolds numbers (25.4°) and is very close to the maximum angle of attack reached during the cycle. C_N max has increased to 2.6 and the loss of lift after stall is very rapid. Recovery from stall does not occur until the minimum angle of attack is reached. In the results for all frequency parameters, the normal force rises rapidly and nonlinearly just prior to stall. This occurs after initial boundary-layer separation (see discussion on pressure distribution) and is probably caused by the increasing strength of the vortex, due to boundary-layer separation, as it forms prior to being shed and convected downstream. Under most test conditions there are several "spikes" in the $C_N - \alpha$ curve just after stall indicating the shedding of more than one vortex.

B. $C_M - \alpha$

For the low-frequency parameter (Fig. 6), pitching moment stall occurs between 16 and 20° angle of attack, depending on Reynolds number. Until the onset of stall, C_M remains zero but then moves rapidly negative as the shed vortex moves back over the wing. Full moment recovery occurs at about 12° angle of attack when C_M returns to zero.

As the frequency parameter is increased to 0.05 (Fig. 7) and 0.065, the angle of moment stall increases but is still Reynolds number dependent. At the highest K (Fig. 8) the angle of moment stall again increases but, as with the angle of lift stall at this K, becomes independent of Reynolds number. Stall occurs at 24° in all cases. Very large, first negative then positve values of $(dC_M/d\alpha)$ occur just after stall producing C_M minimums of -0.5. As with C_N at this high frequency, recovery does not occur before α minimum has been reached.

Moment stall occurs before lift stall. Increasing suction associated with the separating vortex causes large negative pitching moments while normal force is still increasing. Moment recovery occurs later than lift recovery. Vortices shed from the leading edge have a much greater effect on the pitching moment than the normal force so the C_M traces are much more erratic than the C_N traces and the spikes caused by shedding of subsidiary vortices more apparent.

C. $C_P - \alpha$

Raw data traces of the surface pressure variations (Fig. 9, $R_N = 2 \times 10^6$, $K = 0.15$, tunnel 2% open) show that as the upper surface pressures decrease with increasing angle of attack the laminar separation bubble moves forward. The bubble is first apparent at $\alpha = 9°$ as it crosses the port located at $x/c = 0.05$ and by $\alpha = 16.5°$ it has moved forward to port $x/c = 0.0125$. First indications of stall are observed at $x/c = 0.05$ at $\alpha = 23.5°$ (half a degree before the onset of moment stall on the force traces) with a slight loss of suction indicating the start of boundary-layer separation. As the angle of attack continues to increase, the point of boundary-layer separation (as indicated by minima in the pressure traces) moves rapidly forward reaching the nose at $\alpha = 24°$.

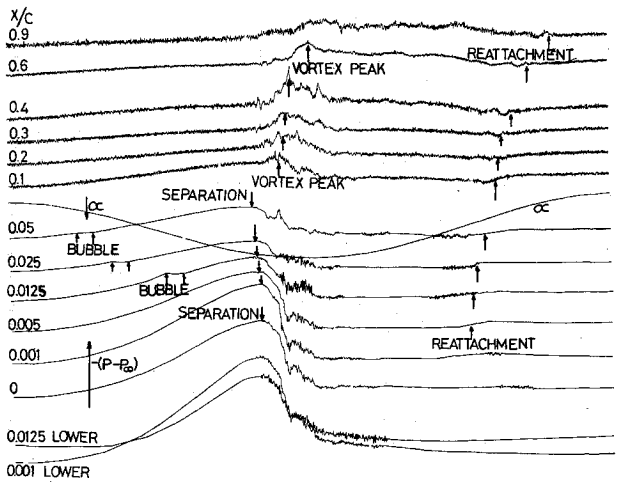

Fig. 9 Data traces of pressure measurements $K=0.15$, $R_N=2\times10^6$.

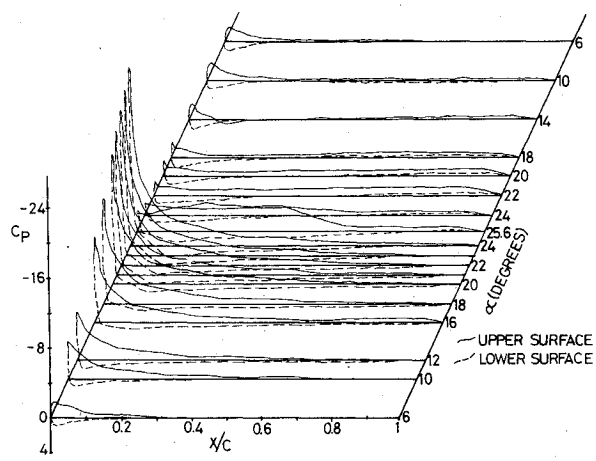

Fig. 10 C_P vs x/c vs $\alpha K=0.15$, $R_N=2\times10^6$.

At $\alpha=24.1°$ the pressure at $x/c = 0.1$ starts to decrease rapidly because the vortex is being formed by the boundary-layer separation which increases in strength. This coincides with the onset of moment stall and the start of the rapid increase in C_N prior to lift stall (Figs. 5 and 8). The pressure at $x/c=0.1$ reaches a minimum at $\alpha=24.7°$, indicating that the vortex has been shed and is moving downstream. Successive minima at port locations aft of $x/c=0.1$ confirm this and show that the vortex moves at about 45% of the fresstream velocity. Smaller suction peaks after the initial minimum indicate the shedding of more than one vortex.

As the onset of boundary-layer separation occurs downstream of the bubble, and subsequently propagates forward toward it, it is apparent that the bubble itself is not the primary trigger mechanism of the stall and that the turbulent boundary layer aft of the bubble separates (as suggested in Ref. 9). Reattachment occurs first near the nose when $\alpha=16$-$19°$ and moves toward the trailing edge at approximately 30% of the freestream velocity reaching $x/c=0.9$ when $\alpha=8.5°$. However, it should be noted that while reattachment of the boundary layer is complete, neither C_N nor C_M recovers until minimum angle of attack has been reached.

Only one case has been discussed, but the data traces for other frequency parameters and Reynolds numbers are similar, differing mainly in the angle of attack at which the stall process starts. When the pressure data are reduced and carpet plotted in the form $C_p - x/c - \alpha$ (Fig. 10 shows the results for $R_N=2\times10^6$, $K=0.15$, and the tunnel 2% open), some of the details previously described (e. g., the forward motion of the bubble prior to stall) are lost because of the scaling required. However, the plots show the build-up of lift to the point of stall and the movement downstream of the suction peak due to the shed vortex after stall.

The general trends noted in the force measurements are clearly indicated, i.e., increasing stall angle with increasing frequency parameter and little effect of the Reynolds number aside from increasing the stall angle at low frequencies. Only minor differences (less than cyclic variations), exist between the closed tunnel and 2% open configuration. One interesting effect is the motion of the forward stagnation point. For the case previously described ($R_N=2\times10^6$, $K=0.15$, tunnel 2% open) the stagnation point starts at $x/c=0.0125$ on the lower surface at α minimum and moves back to about $x/c=0.1$ just prior to the start of stall at $\alpha=24°$. Soon after stall, it moves rapidly forward and by $\alpha=22°$ it is back at $x/c=0.0125$ where it remains for the rest of the cycle. This behavior is qualitatively the same for all the other frequencies tested.

D. Effects of Slotted Walls

In steady flow, there are significant corrections required to data obtained on a 4-ft chord two-dimensional NACA 0012 airfoil in a 7 × 10 ft wind tunnel but they can be reduced considerably by a 2% opening of the tunnel sidewalls[12]. In unsteady flow, at all the frequencies tested, differences in results between closed tunnel and 2% open were smaller than cyclic variations in any one test. Even the stall angles were the "same" for the two configurations. This indicates that in unsteady flow either the 2% opening is insufficient to minimize the corrections, or that the dynamics of the flow about the wing (i. e., the build-up and loss of lift) is such that it is almost equivalent to "free air" conditions. While the author cannot prove the latter it is felt that it is the more probable. The frequencies used, particularly for the low values of K, were so low that the pressure fields on the tunnel walls should respond as though the flow were steady, and therefore the wall porosity required for minimum corrections should be similar to the steady flow case.

Conclusions

Increasing the Reynolds number from 1 × 10^6 to 3 × 10^6 increases the angle of attack at which dynamic stall occurs. This effect decreases with increasing frequency parameter. The Reynolds number does not have any effect on the nature of the stall process, the same type of stall occurs at all Reynolds numbers tested.

Differences between results obtained in a closed tunnel and a tunnel with the sidewalls 2% open were in all cases smaller than the cyclic variations in each test. It appears that the wind-tunnel corrections required for unsteady flow through stall in a closed tunnel are significiantly smaller than those required for steady flow.

The dynamic stall process is not triggered by the bursting of a leading-edge laminar separation bubble; instead the turbulent boundary-layer downstream of the bubble separates first and the separation point moves forward to the bubble. The vortex shed in the stall process moves downstream at about 45% of the freesteam velocity. Boundary-layer reattachment after the stall occurs first near the nose and moves downstream at about 30% of the freestream velocity. Since the stall process starts with a breakdown of the turbulent boundary layer rather than the bursting of a bubble, it might be possible, at least for the two-dimensional case, to develop a theoretical model that will predict the stall characteristics. Any such theoretical approach, however, should allow for the motion of the front stagnation point.

References

[1] Ham, N.D. and Garelick, M.S., "Dynamic Stall Consideration in Helicopter Rotors," *Journal of the American Helicopter Society*, Vol. 13, April 1968, pp. 49-55.

[2] Parker, A.G. and Bicknell, J, "Some Measurements on Dynamic Stall," *Journal of Aircraft*, Vol. 11, July 1974, pp. 371.

[3]Martin, J.M. Empey, R.W., McCroskey, W.J., and Caradonna, F.X., "An Experimental Analysis of Dynamic Stall on Oscillating Airfoil," *Journal of the American Helicopter Society,* Vol. 19, Jan. 1974, pp. 26-30.

[4]Silcox, R.J. and Szwarc, W.J., "Wind Tunnel Dynamic Analysis of an Oscillating Airfoil," AIAA Paper 74-259, Washington D.C., Jan. 1974.

[5]Carta, F.O., "Chordwise Propagation of Dynamic Stall Cells on an Oscillating Airfoil," AIAA Paper 75-25, Pasadena, Calif., Jan. 1975.

[6]Ericsson, L.E. and Reding, J.P., "Dynamic Stall Analysis in the Lit of Recent Numerical and Experimental Results" *Journal of Aircraft,* Vol. 13, April 1976, pp. 248-255.

[7]Johnson, W. and Ham, N. D., "On the Mechanism of Dynamic Stall," *Journal of the American Helicopter Society,* Vol. 17, Oct. 1972, pp. 36-45.

[8]McCroskey, W.J. and Fisher, R.K. Jr., "Detailed Aerodynamic Measurements on a Model Rotor in the Blade Stall Regime," *Journal of the American Helicopter Society,* Vol. 17, Jan. 1972, pp. 20-30.

[9]McCrosky, W.J. Carr, L.W. and McAllister, K.W., "Dynamic Stall Experiments on Oscillating Airfoils," *AIAA Journal,* Vol. 14, Jan. 1976, pp. 57-63.

[10]Pearcey, H.H., Sinnot, C.S.,and Osbourne, J.,"Some Effects of Wind Tunnel Interference Observed in Tests on Two-Dimensional Aerofoils at High Subsonic and Transonic Speeds," AGARD Report 296, March 1959.

[11]Parkinson, G.V. and Lim, A.K.," On the Use of Slotted Walls in Two-Dimensional Testing of Low Speed Airfoils," *CASI Transactions,* Vol. 4, Sept. 1971.

[12]Parker, A.G."Use of Slotted Walls to Reduce Wind-tunnel boundary Corrections in Subsonic Flow," *AIAA Journal,* Vol. 12, Dec. 1974, pp. 1771-1772

[13]McAllister, K.W., private communication, NASA Ames Research Center, Moffett Field, Calif.